INTERNATIONAL JOURNAL FOR NUMERICAL METHODS IN FLUIDS, VOL. 4, 127–145 (1984)

A FINITE-ELEMENT STUDY OF THE BÉNARD PROBLEM USING PARAMETER-STEPPING AND BIFURCATION SEARCH

C. P. JACKSON AND K. H. WINTERS

Theoretical Physics Division, AERE Harwell, Didcot, Oxon, OX11 0RA England

SUMMARY

The problem of fluid motion in a cavity with rigid sidewalls that is heated uniformly from below is studied by the finite-element method. The techniques of parameter-stepping and monitoring the determinant of the Jacobian matrix to find bifurcations are used. Results are presented for width-to-height ratios in the range 1 to 4, and for three different boundary conditions on the horizontal surfaces, namely both rigid, both free, and rigid bottom with free top. The non-linear branches above the critical Rayleigh number are examined. Extensions to non-Boussinesq flow are trivial.

KEY WORDS Finite Element Bénard Connection Bifurcation Continuation

INTRODUCTION

The Bénard problem of the motion of the fluid in a rectangular cavity that is uniformly heated from below is of practical and theoretical importance. It has applications in such diverse branches of physics as meteorology and astrophysics, and it provides a simple example of bifurcations in a fluid flow problem.

The physical phenomena can be summarized as follows. If the Rayleigh number Ra (which is a dimensionless measure of the temperature difference across the cavity) is less than a certain critical value Ra_{crit} then there is no flow and a uniform vertical temperature gradient. If Ra is greater than Ra_{crit} then the no-flow state is unstable, and steady convection cells form. Ra_{crit} and the number of convection cells that form depend upon the width-to-height ratio of the cavity, and upon the boundary conditions upon the walls of the cavity.

The theory of the effect is as follows. At the critical Rayleigh number there is a bifurcation of the solution of the non-linear steady flow equations. If Ra is less than Ra_{crit} then there is only the no-flow solution, whereas if Ra is greater than Ra_{crit} there are (at least) three solutions namely the no-flow solution, and two different senses of flow. This is illustrated schematically in Figure 1. The no-flow solution is unstable as a solution of the time dependent equations if Ra is greater than Ra_{crit}.

If Ra is only slightly greater than Ra_{crit} then the flow velocities are small, and so Ra_{crit} can be obtained from a linear eigenvalue problem derived by neglecting the non-linear terms in the steady flow equations. However, only a very limited number of different boundary conditions can be solved analytically. In particular the case of a finite cavity with rigid walls on all sides requires numerical treatment. A numerical approach is also necessary to obtain the magnitude of the flow for values of Ra greater than Ra_{crit} as it is determined by the neglected non-linear terms.

0271–2091/84/020127–19$01.90

Received 12 July 1982
Revised 25 October 1982

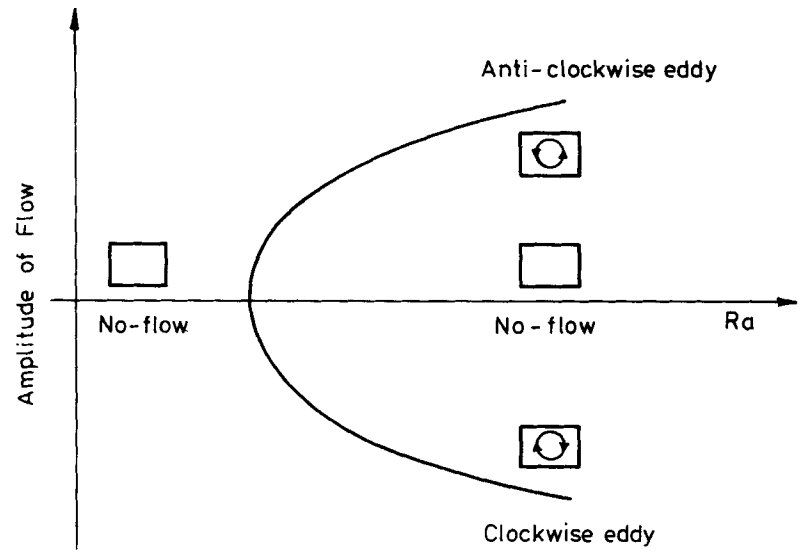

Figure 1. Schematic diagram of the bifurcation in the Bénard problem at Ra_{crit}. The signed amplitude of the flow is plotted against Ra. (The flow on the various branches is indicated by the pictures)

We show here how a standard finite-element program for buoyancy-driven flow can be used to obtain Ra_{crit} as a function of the width-to-height ratio of the cavity, for various different boundary conditions; and also to study the flow at values of Ra greater than Ra_{crit}. The techniques used are parameter-stepping (method of Euler–Newton continuation[1,2]) and bifurcation search by monitoring the determinant of the Jacobian matrix.[2] These are very easy to implement, and extremely cheap to run.

There are considerable advantages to using a standard finite element program rather than a program specially designed for the Bénard problem. It is trivial to change the boundary conditions, and extensions to non-Boussinesq flow are simple. The flow for Ra greater than Ra_{crit} can be studied easily. The method is applicable to studying bifurcations in any field problem, for example flow in an expanding channel.[3]

The numerical results reveal some of the rich structure of the Bénard problem. Comparisons with analytic or semi-analytic solutions, in cases where they exist, show that the method is very accurate.

THE BOUSSINESQ EQUATIONS

The Bénard problem is illustrated in Figure 2. The two-dimensional steady Boussinesq equations for buoyancy-driven flow in the cavity are, in non-dimensional form:

$$\begin{aligned} u\frac{\partial u}{\partial x}+v\frac{\partial u}{\partial y}+\frac{\partial p}{\partial x}-Pr\,\nabla^2 u&=0\\ u\frac{\partial v}{\partial x}+v\frac{\partial v}{\partial y}+\frac{\partial p}{\partial y}-Pr\,\nabla^2 v-RaPrT&=0\\ \frac{\partial u}{\partial x}+\frac{\partial v}{\partial y}&=0\\ u\frac{\partial T}{\partial x}+v\frac{\partial T}{\partial y}-\nabla^2 T&=0 \end{aligned} \qquad (1)$$

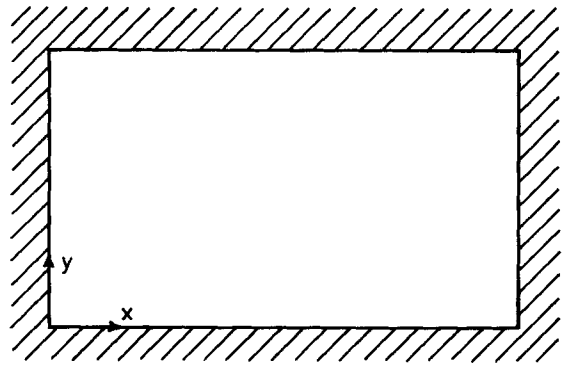

Figure 2. The Bénard problem

for

$$0 \leqslant x \leqslant \beta, \qquad 0 \leqslant y \leqslant 1$$

where u and v are velocity components in the x and y directions, p is pressure, T is temperature, β is the width-to-height ratio of the cavity, Pr is the Prandtl number, and Ra is the Rayleigh number. (In terms of the physical quantities

$$Pr = \frac{\nu}{\kappa}$$

and

$$Ra = \frac{\alpha(\Delta T) g H^3}{\kappa \nu}$$

where ν is the viscosity of the fluid, κ is the thermal diffusion coefficient of the fluid, α is the coefficient of thermal expansion of the fluid, ΔT is the temperature difference across the cavity, g is the acceleration due to gravity, and H is the height of the cavity.)

Throughout the study the sidewalls of the cavity were taken to be rigid. We considered three different sets of boundary conditions on the horizontal walls, namely both rigid, both free, and rigid bottom with free top. (The second of these may seem somewhat artificial, but it actually has relevance to meteorology, and more importantly is more tractable analytically, so that some results exist which can be compared with the present finite-element solution.) On rigid walls both components of velocity were taken to be zero, whereas on free walls the normal component only was taken to be zero. The boundary conditions on temperature are

$$T = 0, \qquad y = 1$$

$$T = 1, \qquad y = 0$$

$$\frac{\partial T}{\partial x} = 0, \qquad x = 0 \quad \text{and} \quad x = \beta$$

Another form of the equations can be obtained by changing variables from x to x^* where

$$x^* = x/\beta$$

The domain of x^*, y is then the unit square and is independent of β, which now appears in the equations instead. For example, the first equation of (1) becomes

$$\beta^{-1} u \frac{\partial u}{\partial x^*} + v \frac{\partial u}{\partial y} + \beta^{-1} \frac{\partial p}{\partial x^*} - Pr\left(\beta^{-2} \frac{\partial^2 u}{\partial x^{*2}} + \frac{\partial^2 u}{\partial y^2}\right) = 0 \tag{2}$$

This formulation has advantages for parameter stepping since the dependence upon the parameter β has been made explicit.

The no-flow state

$$\begin{aligned} u &= 0 \\ v &= 0 \\ p &= RaPr(y - \tfrac{1}{2}y^2) + \text{constant} \\ T &= 1 - y \end{aligned} \tag{3}$$

is always a solution of the equations (1) and the boundary conditions. (It may not be the only one, and indeed we shall show numerically that for Ra greater than Ra_{crit} there are more solutions.)

THE NUMERICAL METHODS

The finite-element method for discretizing equations such as (1) or (2) is standard, and well described elsewhere.[4] We used six-node quadratic triangles to model velocities and temperature, and three-node linear triangles to model pressure, on grids such as that shown in Figure 3. (Mixed interpolation is necessary to ensure that the discrete linear equations for the pressure have a unique solution,[5,6] given the velocities and temperature.)

The finite-element method leads to a set of coupled non-linear algebraic equations for the nodal values of the fields, which can be written

$$F_i(\mathbf{X}; \mathbf{a}) = 0, \qquad 1 \leqslant i \leqslant N \tag{4}$$

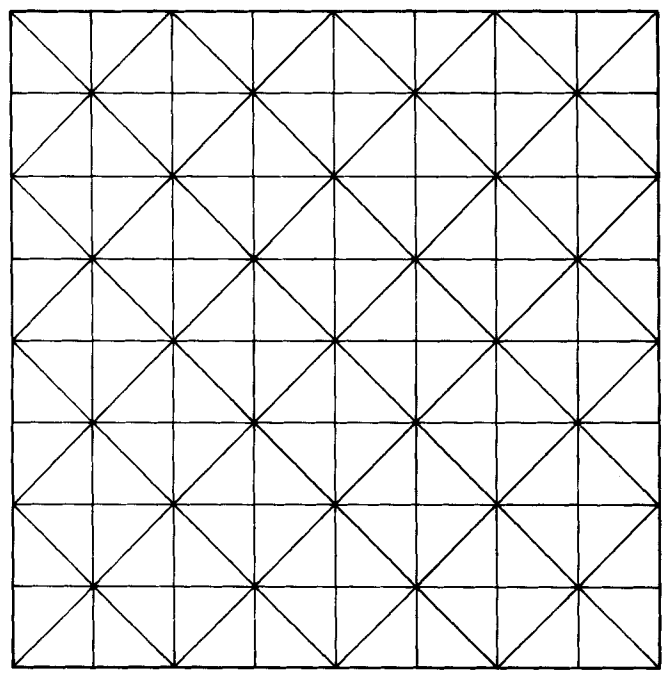

Figure 3. A typical finite-element grid of six-node quadratic triangles used for the study. (The grid is 17×17 in the notation of this paper)

where $\mathbf{X}$ is the vector of unknown nodal field values (of which there are N), and $\mathbf{a}$ is the vector of parameters (including Ra, Pr, and β in the present Bénard study). In order to solve these equations for given parameter values it is necessary to linearize them and iterate. We use the Newton–Raphson method of linearization about the latest estimate, but quasi-Newton–Raphson linearization about an earlier estimate could equally be used. The Newton–Raphson scheme is: choose an initial guess $\mathbf{X}^0$; then solve successively for $\mathbf{X}^1, \mathbf{X}^2, \ldots$, from the linear system

$$\frac{\partial F_i(\mathbf{X}^n; \mathbf{a})}{\partial X_j}(X_j^{n+1} - X_j^n) = -F_i(\mathbf{X}^n; \mathbf{a}) \tag{5}$$

(where we have used the Einstein summation convention). This introduces the Jacobian matrix $\mathbf{J}$ where

$$J_{ij} \equiv \frac{\partial F_i}{\partial x_j}$$

The Newton–Raphson scheme converges quadratically, provided that the initial guess is good enough, whereas the quasi-Newton–Raphson scheme only converges linearly.

We solve the linear system (5) by the (direct) frontal method of Gaussian elimination. $\mathbf{J}$ is decomposed into the product of lower and upper triangular matrices $\mathbf{L}$ and $\mathbf{U}$ as

$$\mathbf{J} = \mathbf{LU} \tag{6}$$

and then equations of the form

$$\mathbf{Jd} = \mathbf{f}$$

are solved by solving successively

$$\mathbf{Le} = \mathbf{f}$$

and

$$\mathbf{Ud} = \mathbf{e}$$

Solving these systems is easy and very cheap, so the cost of the elimination is dominated by the contribution from the $\mathbf{LU}$ decomposition.

The scheme described above has an unexpected bonus. Consider solving (4) for several sets of values $\mathbf{a}_{(1)}, \mathbf{a}_{(2)}, \ldots$, of the parameters $\mathbf{a}$. The cost of finding the solution for given values $\mathbf{a}_{(2)}$ of the parameters is much reduced if the initial guess is good, and an obvious choice is the solution $\mathbf{X}_{(1)}$ at neighbouring values $\mathbf{a}_{(1)}$ of the parameters. An even better guess is

$$X_{(1)i} + \frac{\partial X_{(1)i}}{\partial a_{(1)\alpha}}(a_{(2)\alpha} - a_{(1)\alpha}) \tag{7}$$

and one better still is

$$X_{(1)i} + \frac{\partial X_{(1)i}}{\partial a_{(1)\alpha}}(a_{(2)\alpha} - a_{(1)\alpha}) + \frac{1}{2}\frac{\partial^2 X_{(1)i}}{\partial a_{(1)\alpha}\partial a_{(1)\beta}}(a_{(2)\alpha} - a_{(1)\alpha})(a_{(2)\beta} - a_{(1)\beta}) \tag{8}$$

and so on.

Now from (4)

$$\frac{\partial F_i}{\partial X_j}\frac{\partial X_j}{\partial a_\alpha} + \frac{\partial F_i}{\partial a_\alpha} = 0 \tag{9}$$

Thus $(\partial X_j/\partial a_\alpha)$ is determined by a linear system with the same matrix $\mathbf{J}$ as in (5), but a different right-hand side, and so once the solution $\mathbf{X}$ for given values $\mathbf{a}$ of the parameter has

been determined ($\partial X_j/\partial a_\alpha$) can be found very cheaply, since it is not necessary to repeat the **LU** decomposition of **J**. (Further, by differentiating (9) with respect to a, it can be seen that ($\partial^2 X_j/\partial a_\alpha\, \partial a_\beta$), and higher derivatives, are also determined by linear systems with the same matrix **J** and so can be calculated very cheaply.)

It is thus possible to obtain a very good initial guess for the solution at parameter values $\mathbf{a}_{(2)}$, once the solution at values $\mathbf{a}_{(1)}$ is known. We have only used (7), but (8) may be better still. Now in many non-linear problems it may not be possible, at some values $\mathbf{a}_{(n)}$ of the parameters, to find, *a priori*, a good-enough initial guess for the Newton–Raphson iterations to converge. However if it is possible to calculate the solution at one set of values $\mathbf{a}_{(0)}$, then by stepping through the solutions at a series of values between $\mathbf{a}_{(0)}$ and $\mathbf{a}_{(n)}$, a good enough initial guess can be obtained. This is Euler–Newton continuation in a parameter.[1,2]

Parameter stepping can be implemented in many ways. The length of the step may be fixed by the user (either as a constant, or as a specified sequence of values) or some form of automatic choice of step size (as in Gear's method for solving stiff systems of ordinary differential equations) can be incorporated into the program. A flow chart for one such automatic method is given in Figure 4. The step length is chosen to be as large as possible consistent with rapid convergence of the Newton–Raphson iterations. The convergence rate of the iterations is estimated from the iterations at previous parameter values, as is the error in the 'predictor' (7), and an appropriate step size is chosen. (It can be shown that, if the initial guess is good enough, then the successive errors Δ_n in the Newton–Raphson iterates behave like

$$\Delta_n = k(\Delta_{n-1})^2$$

where k is a constant, and so successive errors are

$$\Delta_0,\ k\Delta_0^2,\ k(k\Delta_0^2) = k^3\Delta_0^4, \ldots,$$

or

$$cr,\ cr^2,\ cr^4,\ cr^8, \ldots,$$

where

$$c = k^{-1},$$
$$r = k\Delta_0 = \Delta_0/c$$

This is used to calculate the convergence rate of the iterations.)

The algorithm given in Figure 4 for the choice of Δa was designed to keep the convergence rate r for the solution at each parameter value approximately equal to 0·1, thus giving convergence to four significant figures in three Newton iterations. We found the algorithm to behave well in practice.

The scheme described in detail above makes it possible to study very cheaply the behaviour of the solution to (4) as a function of the parameters.

At first sight there might seem to be a problem if there are any bifurcations in the solution, but in practice the initial guess obtained by parameter-stepping is so good that there is usually no problem in following one branch, just stepping past bifurcations as illustrated schematically in Figure 5.

Further, and most importantly, it is actually possible to locate the position of any bifurcations on the branch by monitoring the determinant[2] of the Jacobian **J**. At bifurcations (and limit points) **J** becomes rank deficient, which gives rise to a zero of det $|\mathbf{J}|$. Thus, provided that the zero is simple, it is easy to locate bifurcations by observing the sign of det $|\mathbf{J}|$, which differs on opposite sides of the bifurcation. Now det $|\mathbf{J}|$ is very easily evaluated because from (6)

$$\det|\mathbf{J}| = (\det|\mathbf{L}|)(\det|\mathbf{U}|)$$

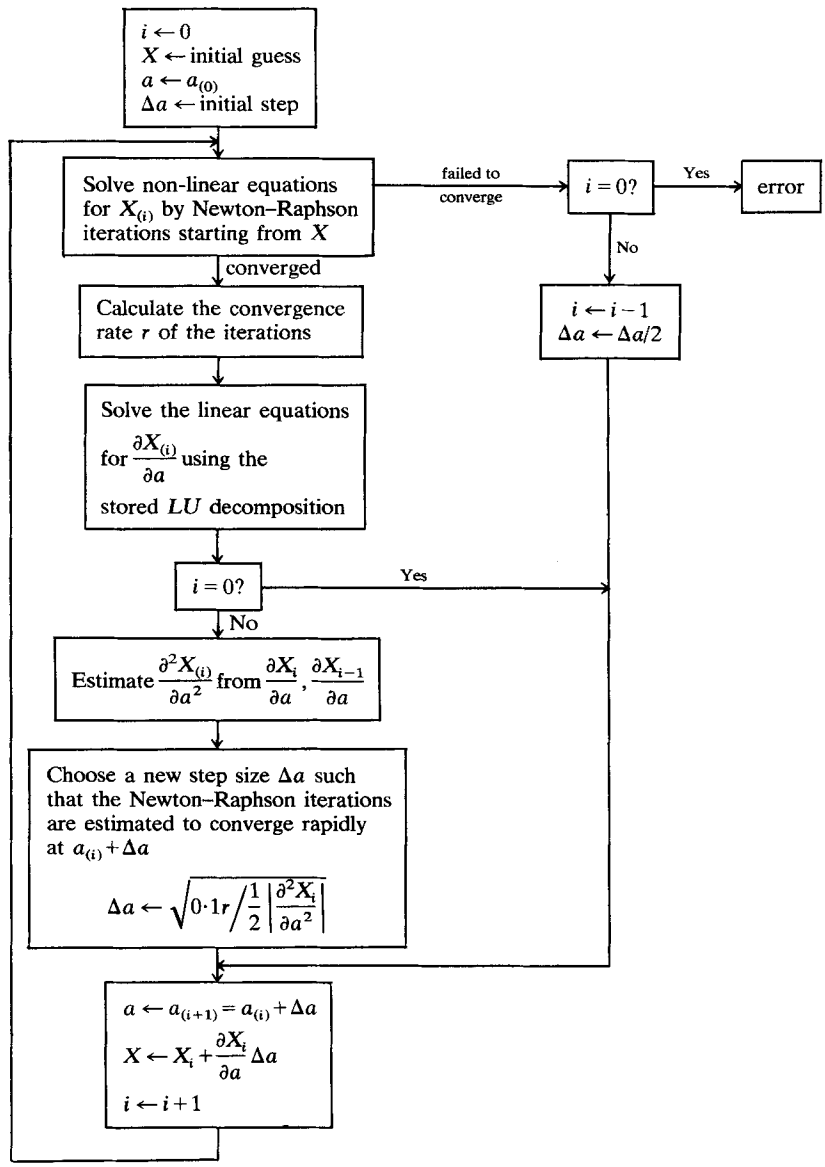

Figure 4. Flow chart for an automatic step-length choice algorithm

and, since **L** and **U** are triangular matrices, their determinants are just the products of their diagonal entries. (If pivoting is used in the **LU** decomposition then this introduces a sign factor which is easily calculated.) In practice the numbers involved are so large that we calculate the sign of $\det|\mathbf{J}|$, and the logarithm of the absolute value of $\det|\mathbf{J}|$.

Thus using the above techniques it is possible to follow the behaviour of the solution as a parameter changes, and to locate any bifurcations. One further technique needs to be

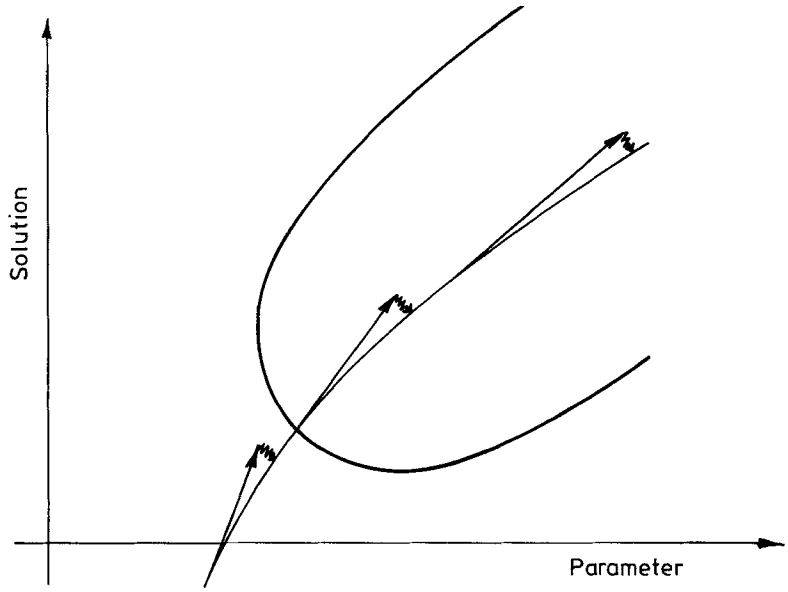

Figure 5. Schematic diagram of parameter stepping, showing its ability to step past bifurcations. The lines — indicate the predictor steps using (7), and the lines ~~ indicate the Newton–Raphson steps

introduced. The solutions on the other branches at a bifurcation can be found as follows. The equations (4) are perturbed slightly, for example to

$$F_i(\mathbf{X}; \mathbf{a}) - \varepsilon F_i(\mathbf{X}^*; \mathbf{a}) = 0 \tag{10}$$

for some $\mathbf{X}^*$ and small ε. Then the structure of the solutions near the bifurcation changes to that illustrated in Figure 6, and parameter-stepping with small step sizes will follow the solution onto a perturbation of one of the other branches. Once sufficiently far from the

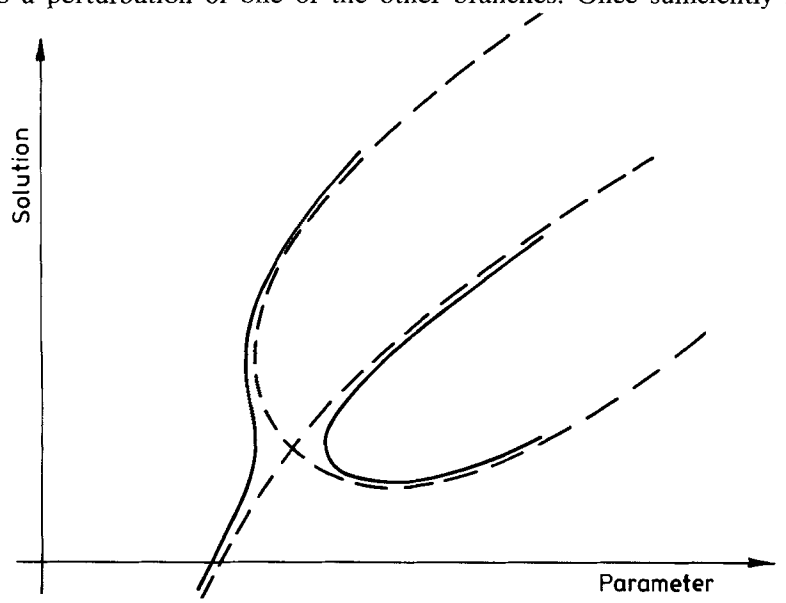

Figure 6. Schematic diagram showing the effect of the perturbation (10) on the bifurcation. The unperturbed bifurcation is shown dashed

bifurcation, ε can be set to zero and the branch followed properly. The other branch can of course be found with an initially negative ε. Any choice of ε and $\mathbf{X}^*$ that perturbs the equations and destroys the bifurcation is adequate, although of course if ε is made too small then many very small steps are needed to follow the solution onto a perturbation of one of the branches.

One final remark can be added. It can be shown[7] that an eigenvalue with negative real part of $\mathbf{J}$ for the steady state equations corresponds to instability of the solution as a solution of the time-dependent equations. Since $\det|\mathbf{J}|$ is just the product of the eigenvalues of $\mathbf{J}$, then it is easy to see that there is at least one negative eigenvalue of $\mathbf{J}$ if $\det|\mathbf{J}|$ is negative, and so the solution is unstable. If $\det|\mathbf{J}|$ is positive then it is not possible to say that there are no eigenvalues of $\mathbf{J}$ with negative real part, (as there may be an even number of such eigenvalues of course). Thus, in regions where $\det|\mathbf{J}|$ is positive, further analysis is needed to determine whether or not the solution is unstable or stable.

RESULTS AND REMARKS

We used the above techniques to study the bifurcations from the no-flow solution in the Bénard problem. (Note that, contrary to the conclusions of Reference 8, we experienced no difficulty in using piecewise-linear basis functions for pressure, even though the analytic pressure in the no-flow state is quadratic. The finite-element method gave a good approximation to the analytic solution without any problems.)

First, we illustrate the method of bifurcation search by monitoring the determinant of the Jacobian matrix. We present in Table I values of the sign, absolute value and logarithm of the absolute value of $\det|\mathbf{J}|$ at various Ra, for the no-flow solution to the Bénard problem with rigid walls on all sides, and width-to-height ratio 1, on a 9×9 grid. (We use the convention that an $M\times N$ grid has M nodes horizontally and N nodes vertically.) It is easy to see that there are bifurcations between $Ra=2650$ and $Ra=2700$ and between $Ra=7000$ and $Ra=8000$. (The negative sign of $\det|\mathbf{J}|$ shows that the no-flow state must be unstable between $Ra=2700$ and $Ra=7000$.) Values of $\det|\mathbf{J}|$ versus Ra for values of Ra between 2400 and 2700 are shown in the graph of Figure 7. It is possible to locate the position of the bifurcation by interpolation between values of $\det|\mathbf{J}|$ on either side of the bifurcation, leading to the value 2652. This corresponds to Ra_{crit}, of course.

Table I. $\det|\mathbf{J}|$ versus Ra for the rigid/rigid case, width-to-height ratio 1, on a 9×9 grid

Ra	sign $\det\|\mathbf{J}\|$	log ($\det\|\mathbf{J}\|$)	$\det\|\mathbf{J}\|$
10	+	72·2	$2{\cdot}19\times10^{31}$
100	+	72·1	$2{\cdot}04\times10^{31}$
2400	+	68·7	$6{\cdot}89\times10^{29}$
2500	+	68·2	$3{\cdot}94\times10^{29}$
2650	+	63·1	$2{\cdot}44\times10^{27}$
2700	−	66·9	$-1{\cdot}15\times10^{29}$
3000	−	68·7	$-6{\cdot}97\times10^{29}$
5000	−	69·3	$-1{\cdot}29\times10^{30}$
7000	−	66·5	$-7{\cdot}29\times10^{28}$
8000	+	68·2	$4{\cdot}29\times10^{29}$
10,000	+	69·0	$9{\cdot}11\times10^{29}$

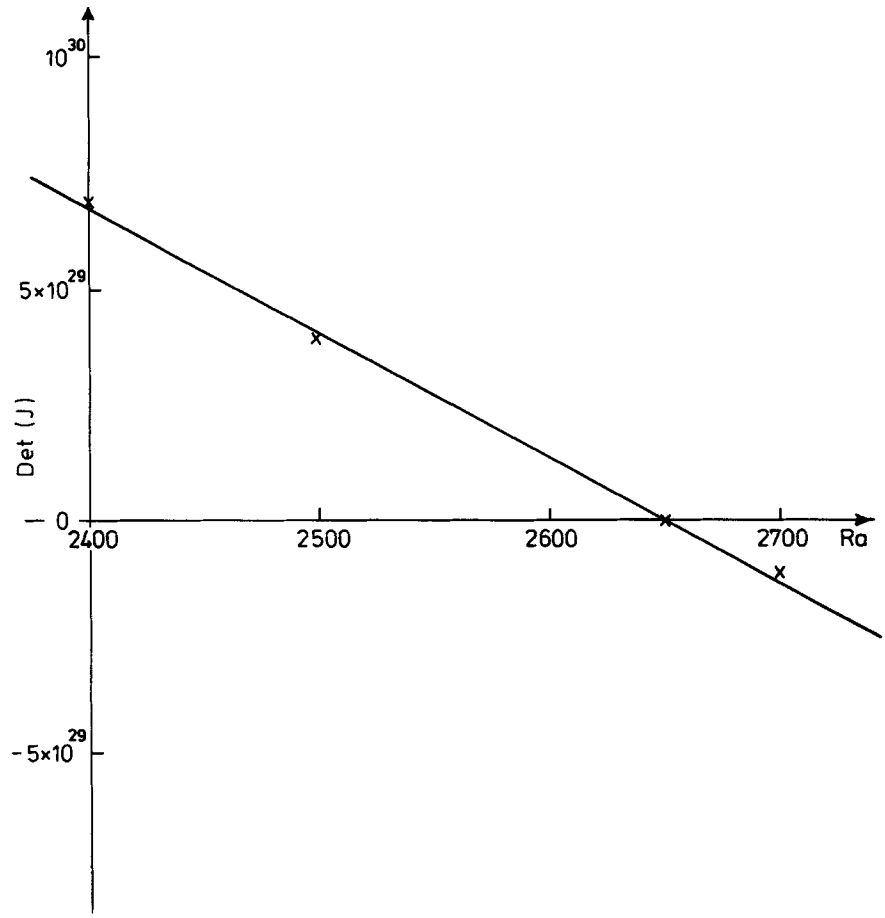

Figure 7. Det |J| versus Ra for the rigid/rigid case, for width-to-height ratio 1, on a 9×9 grid, for Ra in the range 2400 to 2700. The straight line is a fit by eye to the values

The calculation was repeated on a 17×17 grid in order to check the dependence of the bifurcation value on the grid spacing. The first bifurcation on a 17×17 grid was at $Ra = 2612$. Thus a quite coarse mesh produced very accurate results.

The technique described at the end of the previous section was used to perturb the solution onto the other branches. (A perturbation of the form suggested in (10) was used, with $\varepsilon = 0{\cdot}01$ and $\mathbf{X}^*$ corresponding to a velocity field of order 1, which was neither even nor odd). The other branches leading from the bifurcation at $Ra = 2650$ were thereby identified as one-cell solutions, and the other branches leading from the bifurcation at $Ra = 7128$ were identified as two-cell solutions.

Figure 8 shows streamlines for the one-cell solution at $Ra = 10{,}000$ on a 17×17 grid and Figure 9 shows the isotherms. Figure 10 shows the streamlines for the two-cell solution at $Ra = 10{,}000$ on a 17×17 grid and Figure 11 shows the isotherms.

Figure 12 shows a graph of the square of the amplitude of the one-cell solution on a 9×9 grid, (measured by the Euclidean norm of the nodal velocity values) plotted against Ra. According to theory this should be a straight line in the neighbourhood of the bifurcation. As can be seen the graph is linear over a very large region.

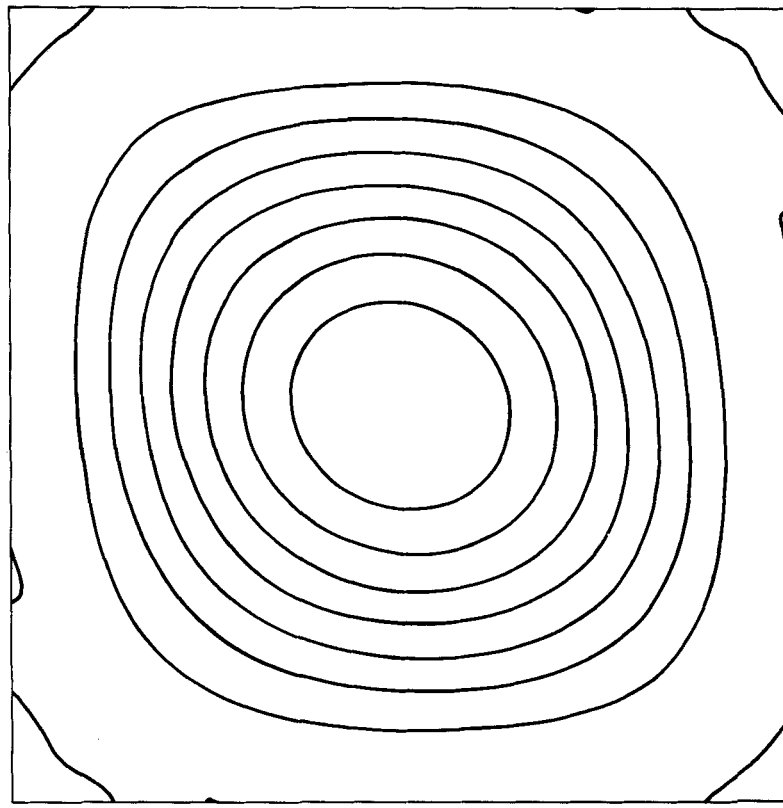

Figure 8. Streamlines for the one-cell solution on $Ra = 10{,}000$ on a 17×17 grid for the rigid/rigid case, at width-to-height ratio 1

Once we had established the feasibility of the method we used it to make a detailed study of the Bénard problem with rigid side walls for width-to-height ratios in the range 1 to 4, and for the three different boundary conditions of rigid top and bottom, free top and bottom, and rigid bottom with free top. The bifurcations from the no-flow branch were determined as above, by monitoring $\det |\mathbf{J}|$ on this branch. The results are presented in Table II and Figure 13 for the rigid/rigid case; in Table III and Figure 14 for the free/free case; and in Table IV and Figure 15 for the rigid/free case.

Results of Luijkx and Platten[9] for the rigid/rigid case and Hall and Walton[10] for the free/free case are also presented for comparison.

At various width-to-height ratios the flow was triggered in the manner described above, and the number of convection cells determined. As the width-to-height ratio is increased the lowest bifurcation value of Ra changes from a branch corresponding to a one-cell solution to a branch corresponding to a two-cell solution, and then to a branch corresponding to a three-cell solution, and so on. The separation between the minima of the various branches is nearly constant for each boundary condition. This implies that there is a preferred convection cell width which is approximately 1·02 for the rigid/rigid case, 1·18 for the rigid/free case, and 1·58 for the free/free case. The analytic values for an infinite width-to-height ratio are 1·02, 1·17 and 1·42, respectively.

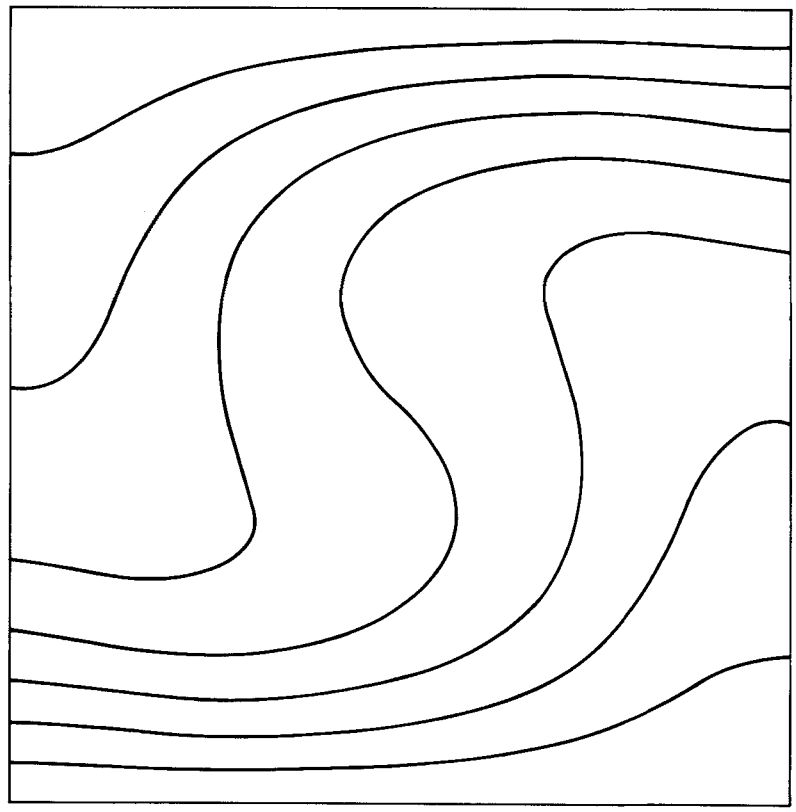

Figure 9. Isotherms for the one-cell solution of Figure 8

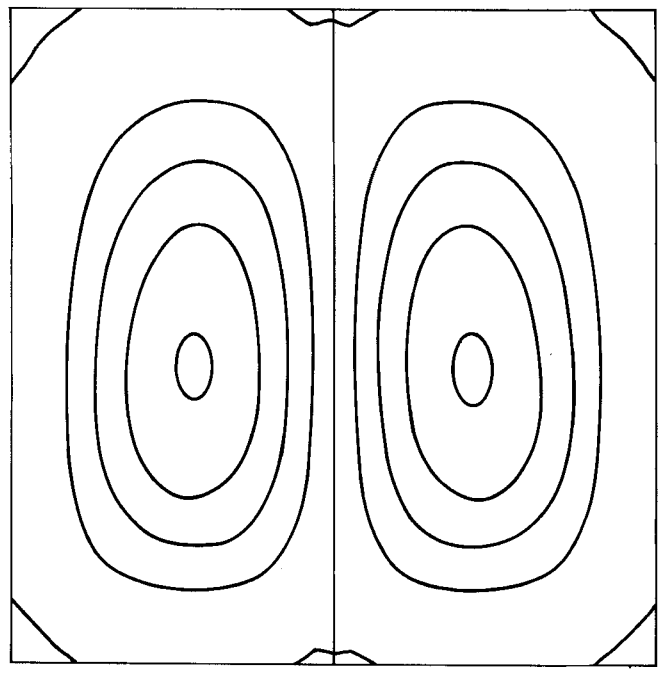

Figure 10. Streamlines at $Ra = 10{,}000$ for the two-cell solution on a 17×17 grid for the rigid/rigid case, at width-to-height ratio 1

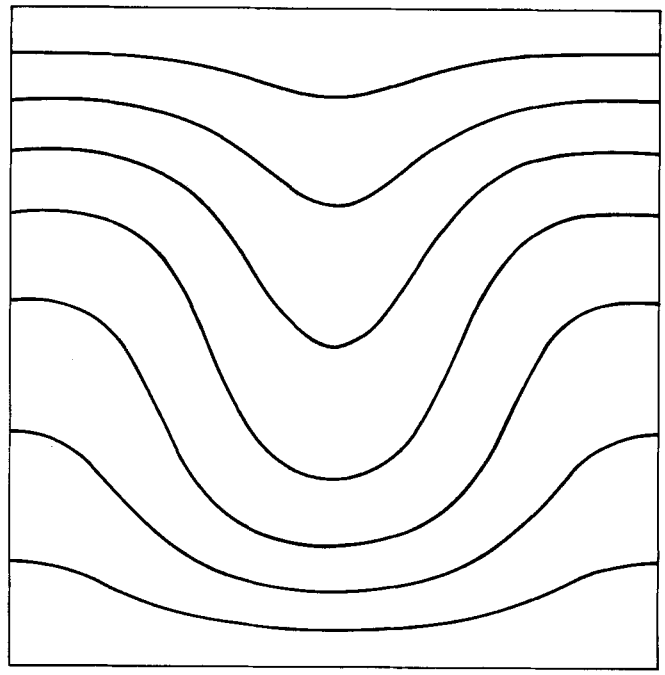

Figure 11. Isotherms for the two-cell solution at $Ra = 10{,}000$ on a 17×17 grid for the rigid/rigid case, at width-to-height ratio 1

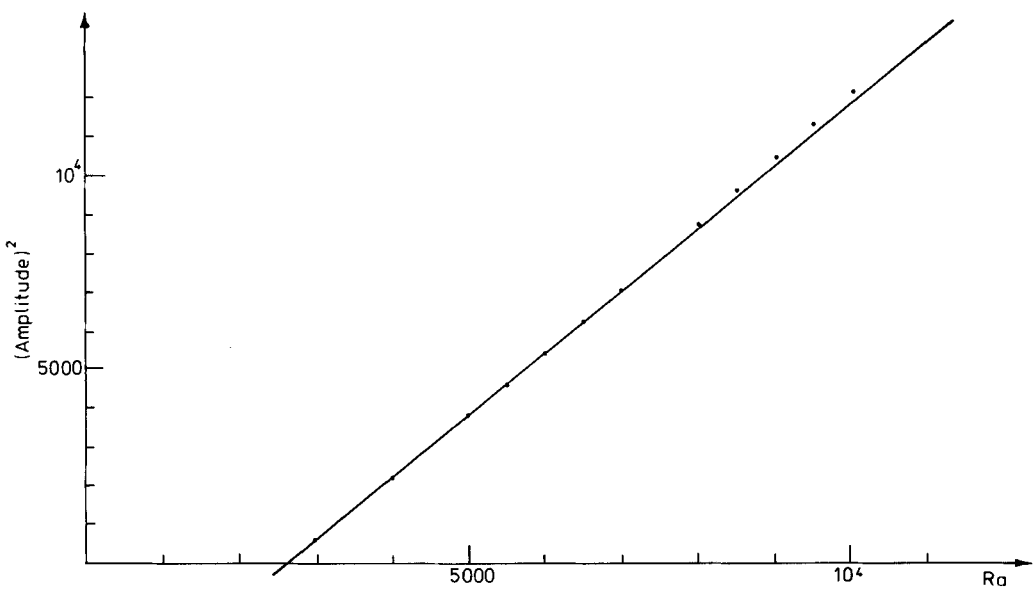

Figure 12. The square of the amplitude of the solution (measured by the Euclidean norm of the velocities) versus Ra for the one-cell solution in the rigid/rigid case at width-to-height ratio 1. Below $Ra = 7000$ the values are indistinguishable from the straight line fit to the values just above $Ra_{crit} \simeq 2600$

Table II. Lowest few bifurcation values of Ra for the rigid/rigid case

Width-to-height Ratio	Grid	Bifurcation values of Ra			
1·0	5×5	3091	9812	16,139	41,223
1·0	9×9	2665	7130	21,406	25,032
1·0	17×17	2588	6774		
1·0	21×21	2612	6491		
1·2	9×9	2353	4432	11,684	
1·4	9×9	2332	3190	7286	
1·6	9×9	2438	2564	5039	
1·6	17×9	2434	2471	5027	
1·6	33×9	2433	2462		
1·8	9×9	2227	2588	3829	
1·8	17×9	2218	2591	3917	
1·8	33×9	2202	2583		
1·9	17×9	2122	2653	3607	
2·0	9×9	2049	2563	3372	
2·0	17×9	2056	2650	3461	
2·0	33×9		2629	3427	
2·2	9×9	1961	2250	3534	
2·2	17×9	1988	2453	3573	
2·4	9×9	1947	1956	3882	
2·4	17×9	1976	2236	3509	3882
2·6	9×9	1740	1942		
2·6	17×9	2000	2079	3022	4095
2·8	9×9	1576	1981		
2·8	17×9	1978	2038	2696	
3·0	9×9	1450			
3·0	17×9	1916	2071	2504	
3·0	33×9	1901	2060		
3·2	33×9	1872	2038		
3·4	33×9	1866	1977		
3·6	33×9	1875	1917		
3·8	33×9	1874	1891		
4·0	33×9	1844	1908		

As the width-to-height ratio β was increased and the number of convection cells at the critical Rayleigh number increased, then it became necessary to increase the number of nodes in the horizontal direction to obtain accurate results. This is hardly surprising since a 9×9 grid cannot be expected to support a solution with a large number of cells.

The results are in remarkable agreement with other numerical results, and such analytic results as exist. The error is typically 1 per cent for Ra_{crit} (which corresponds to the lowest bifurcation of course). The following observation explains this accuracy. As already stated, the critical Rayleigh number, which is a bifurcation from the no-flow state, can be obtained from a linear eigenvalue problem. In a roundabout fashion the finite element method is making a Rayleigh–Ritz approximation for this problem, and this is well known to give a second-order-accurate approximation to the lowest eigenvalue. One would not expect quite such accuracy from a coarse grid when studying bifurcations for a truly non-linear problem, as the grid has to be fine enough to adequately represent the non-linear solution.

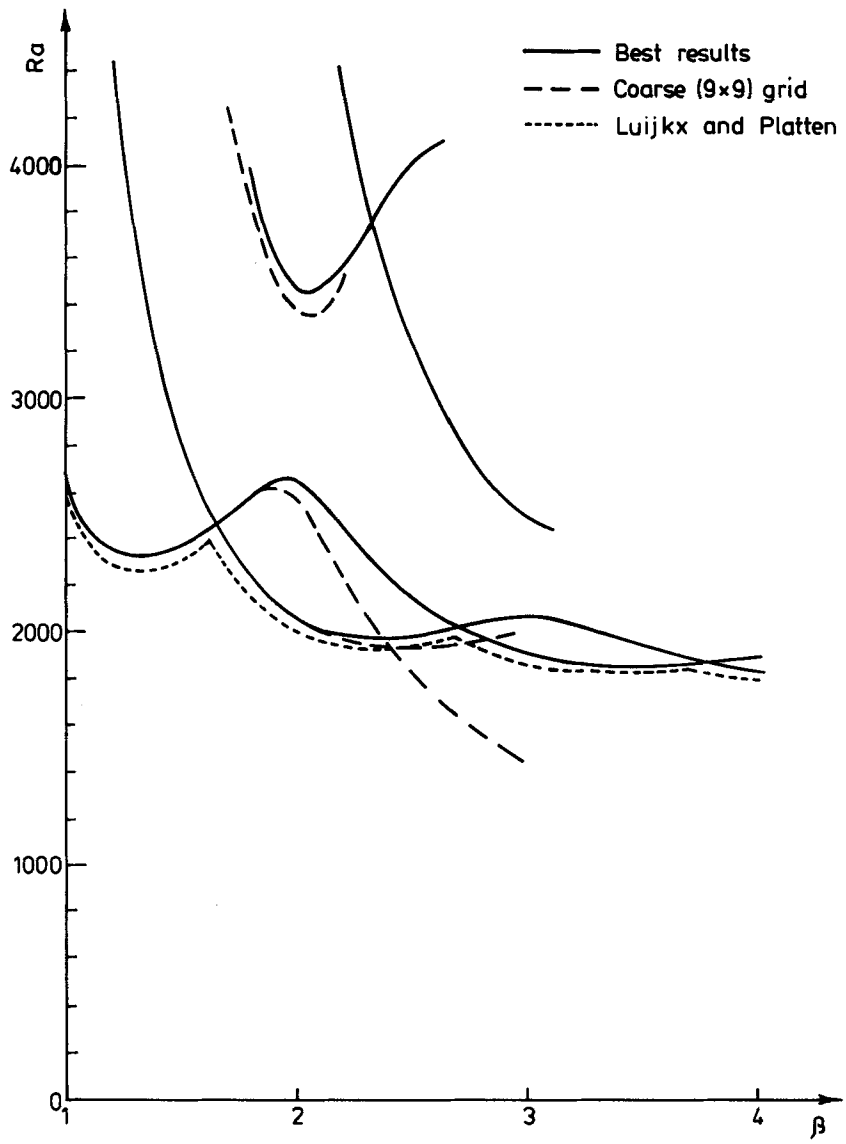

Figure 13. Bifurcation values versus width-to-height ratio for the rigid/rigid case

One feature of our results deserves comment. We expected that the bifurcation diagrams should be as shown in Figure 16. However the curves in the encircled area do not cross in practice but are as shown in the insert. We believe that this may be due to discretization error breaking the degeneracy of the solutions (of the same parity) at the cross-over point, but we were unable to verify this. Although refining the grid by a factor of two in both directions changed the curves slightly the gap remained much the same.

Finally, we used parameter-stepping to follow the non-linear branch from the second

Table III. Lowest few bifurcation values of Ra for the rigid/free case

Width-to-height ratio	Grid	Bifurcation values of Ra		
1·0	9×9	2081	6654	19,252
1·2	9×9	1671	3966	11,269
1·4	9×9	1525	2722	6911
1·6	9×9	1504	2074	4672
1·8	9×9	1544	1707	3414
2·0	9×9	1498	1620	2673
2·0	17×9	1485	1616	2669
2·2	17×9	1362	1683	2302
2·4	17×9	1300	1642	
2·6	17×9	1272	1523	
2·8	17×9	1268	1415	
3·0	17×9	1278	1333	
3·0	33×9	1244	1320	
3·2	33×9	1266	1291	
3·4	33×9	1229		
3·6	33×9	1207	1311	
3·8	33×9	1198	1286	
4·0	33×9	1196	1253	

Table IV. Lowest few bifurcation values of Ra for the free/free case

Width-to-height ratio	Grid	Bifurcation values of Ra			
1·0	9×9	1705	6276	14,262	18,617
1·2	9×9	1233	3613	10,919	
1·4	9×9	1026	2379	6598	12,600
1·6	9×9	931	1730	4382	
1·8	9×9	897	1357	3132	
2·0	17×9	894	1100	2269	
2·1	17×9	905	1026	2022	
2·2	17×9	927	955	1824	
2·3	17×9	—	—	1665	
2·4	17×9	882	947	1538	
2·5	17×9	848	965	1439	
2·5	33×9	—	962	1422	
2·6	17×9	820	976	1367	
2·66	17×9	808	979	1336	
2·74	17×9	794	977	1310	
2·8	17×9	785	970	1301	
2·9	17×9	773	951	1304	
3·0	17×9	764	926		
3·0	33×9	760	918		
3·2	33×9	751	865		
3·3657	33×9	750	827		
3·6	33×9	756	786		
3·8	33×9	—	—		
4·0	33×9	738	770		

The —s indicate places where two bifurcation values were too close to be resolved separately, or where the range containing a bifurcation was not scanned with a particular grid

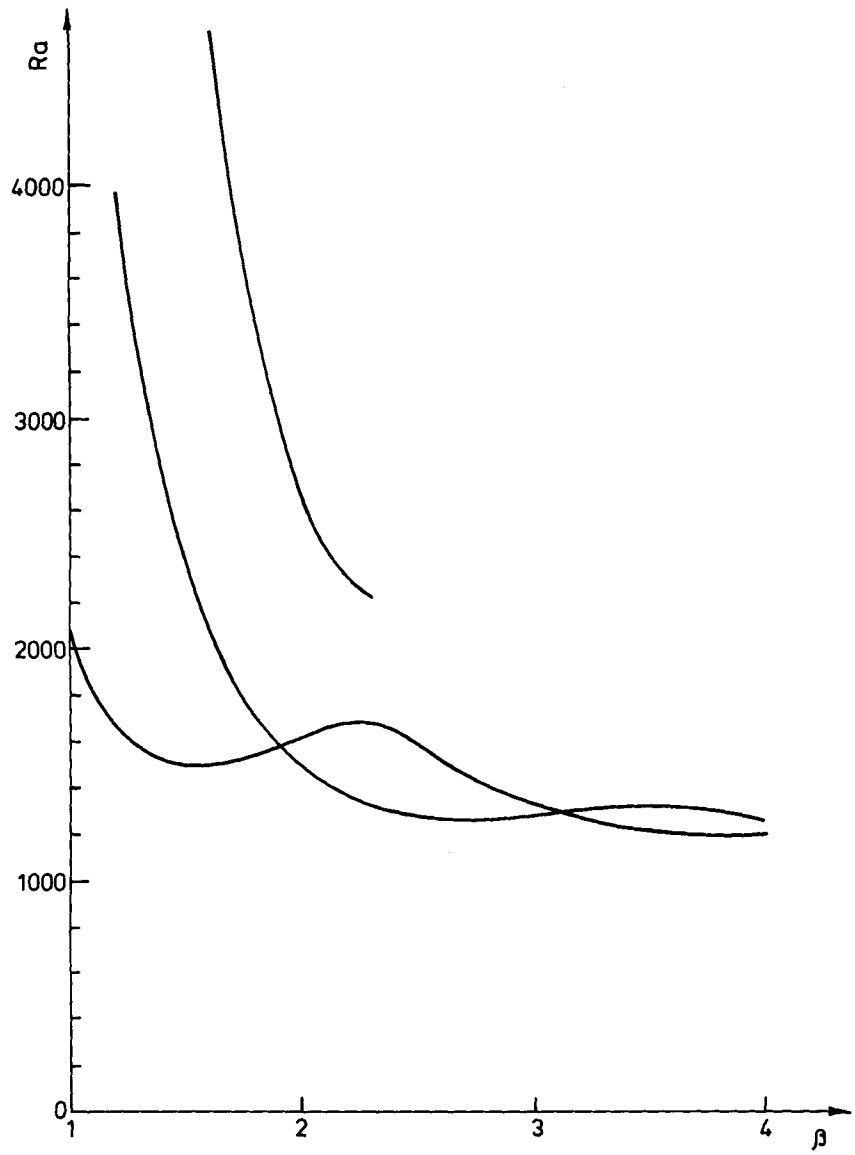

Figure 14. Bifurcation values versus width-to-height ratio for the free/free case

bifurcation in the rigid/rigid case with width-to-height ratio 1, on a 9×9 grid, from the bifurcation at $Ra = 7128$ up to a limit point at $Ra = 29{,}000$ approximately. There is no physical significance to be attached to this limit point. It is simply a consequence of the inability of the very coarse grid to adequately model the boundary layers as the flow velocities increase. However it does illustrate the potential of the method for finding physical limit points if they exist.

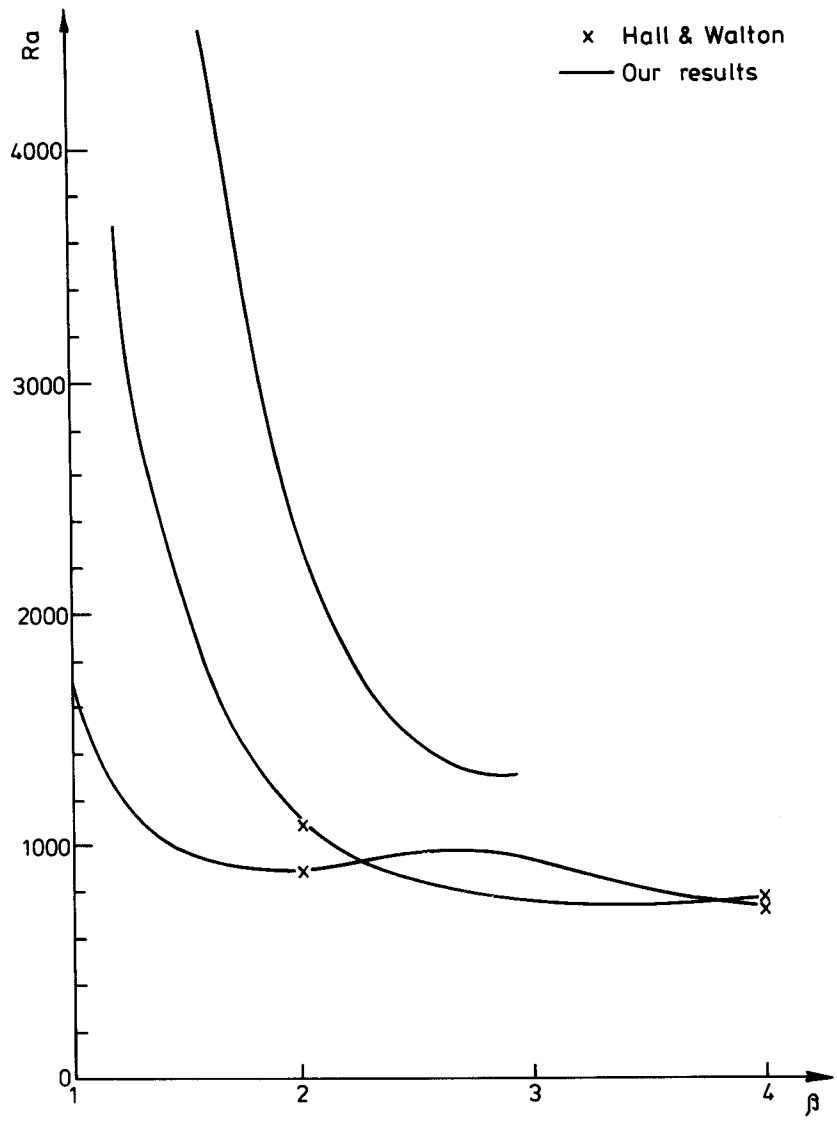

Figure 15. Bifurcation values versus width-to-height ratio for the rigid/free case

CONCLUDING REMARKS

The results presented here for the Bénard problem show some of the power and flexibility of the techniques of parameter-stepping and bifurcation search. Since the methods are based upon a general finite-element program they can be easily applied to study bifurcations in any field problem. For example the Bénard problem could be studied without making the Boussinesq approximation. The techniques are being used to study a bifurcation in diverging channel flow.[3]

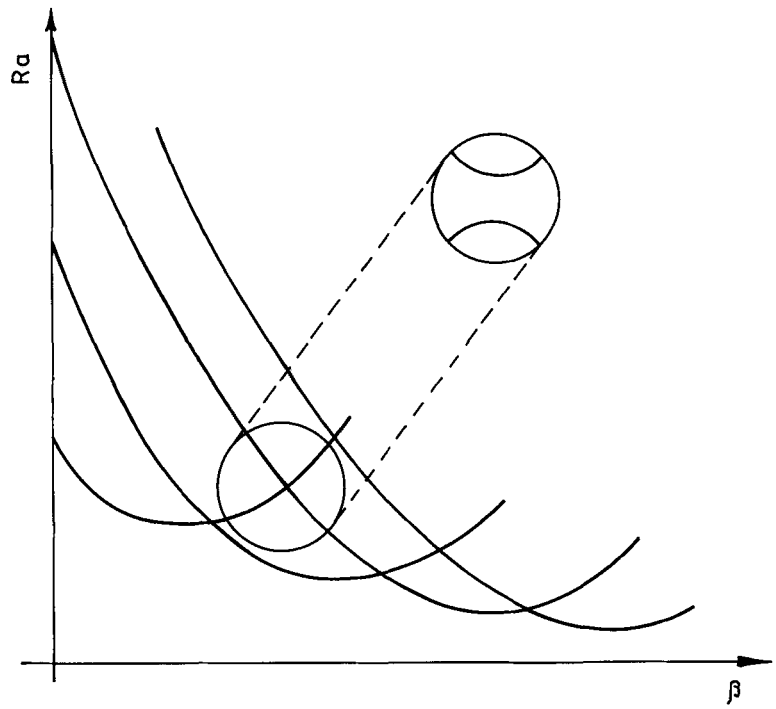

Figure 16. Expected plot of bifurcations versus width-to-height ratio. The insert shows the actual behaviour in the encircled region

REFERENCES

1. D. F. Davidenko, *Dokl. Acad. Nauk, SSSR*, **88,** 601–602 (1953).
2. H. B. Keller, 'Numerical solution of bifurcation and non-linear eigenvalue problems', *Applications of Bifurcation Theory*, Academic Press, 1977.
3. K. A. Cliffe and A. C. Greenfield, 'Some comments on laminar flow in symmetric two-dimensional channels' *AERE Harwell Report, AERE-TP939* (1982).
4. O. C. Zienkiewicz, '*The Finite-Element Method*', McGraw-Hill.
5. C. P. Jackson and K. A. Cliffe, Mixed interpolation in primitive variable finite-element formulations for incompressible flow', *Int. J. Num. Meth. Eng.*, **17,** 1659–1688 (1981).
6. R. L. Sani, P. M. Gresho, R. L. Lee and D. F. Griffiths, *Int. J. Num. Meth. Fluids*, **1,** 17–43 (1981) and R. L. Sani, P. M. Gresho, R. L. Lee, D. F. Griffiths and M. S. Engelman, *Int. J. Num. Meth. Fluids*, **1,** 171–204 (1981).
7. K. A. Cliffe, private communication (1982).
8. J. C. Van Steeg and P. Wesseling, 'Solution of the Boussinesq equations by means of the finite-element method', *Computers and Fluids*, **6,** 93–101 (1978).
9. J. Luijkx and J. K. Platten, 'On the onset of free convection in a rectangular channel', *J. Non-Equilib. Thermodyn.*, **6,** 141–158 (1981).
10. P. Hall and I. C. Walton, 'The smooth transition to a convective region in a two-dimensional box', *Proc. Roy. Soc. Lond. A*, **358,** 199–221 (1977).